

Article

Response of Seismically Damaged Steel Reduced Beam Section Joints under Fire

Roberto Tartaglia ^{1,*} , Mario D'Aniello ²  and Raffaele Landolfo ²¹ Department of Engineering (DING), University of Sannio, 82100 Benevento, Italy² Department of Structures for Engineering and Architecture, University of Naples Federico II, 80131 Naples, Italy

* Correspondence: rotartaglia@unisannio.it

Abstract: The behaviour of seismically damaged steel joints with reduced beam section (RBS) at elevated temperatures has not been widely investigated yet. Therefore, the study summarized in this article aimed to (i) analyse the response of RBS joints at high temperatures and (ii) investigate the influence of plastic damage, due to cyclic loading, on the fire performance of the joints. A set of RBS joints with rib stiffeners on the both lower and upper beam flanges was designed according to European standards and the following parameters were considered: (i) location of the joint (i.e., internal or external joint) and (ii) reduction in the beam flexural resistance (i.e., 65% or 80% of the beam plastic moment). The mechanical response of these joints was simulated by means of finite element models (FEM). The accuracy and effectiveness of the adopted modelling assumptions to mimic the seismic response of the joints were validated against experimental results available from the existing literature. The numerical results highlight that under cyclic loading, all investigated joints exhibit ductile behaviour, allowing the concentration of the plastic deformation within the reduced segment of the beam. The designed reduction in the beam flexural resistance influences the joint fire performance, being impaired in the cases with lower flexural resistance. In contrast, the imposed cyclic pre-damage does not appreciably affect the fire resistance of the investigated joints.

Keywords: steel joint; cyclic behaviour; elevated temperature; reduced beam section; fire; finite element analysis



Citation: Tartaglia, R.; D'Aniello, M.; Landolfo, R. Response of Seismically Damaged Steel Reduced Beam Section Joints under Fire. *Appl. Sci.* **2023**, *13*, 3641. <https://doi.org/10.3390/app13063641>

Academic Editor: Dario De Domenico

Received: 21 February 2023

Revised: 2 March 2023

Accepted: 9 March 2023

Published: 13 March 2023



Copyright: © 2023 by the authors. Licensee MDPI, Basel, Switzerland. This article is an open access article distributed under the terms and conditions of the Creative Commons Attribution (CC BY) license (<https://creativecommons.org/licenses/by/4.0/>).

1. Introduction

Fire after a major earthquake is an extreme event that has occurred many times with devastating effects [1,2]. Steel structures are generally sensitive to fire due to the intrinsic limited thermal inertia, and their fire resistance can be significantly reduced if seismically damaged, as also shown by [1–3]. In fact, steel moment-resisting frames (MRFs) can dramatically lose their lateral rigidity and resistance following major earthquakes if plastic hinges form in the columns. Nowadays, capacity design rules are widely used to enforce the plastic deformations at the ends of the beams of MRFs, provided that the beam-to-column joints guarantee adequate ductility [4–6]. Many types of beam-to-column joints have been studied, verified and used in many applications [7]. Among them, dog-bone or reduced beam section (RBS) moment-resisting joints are brilliant solutions to decrease the demand on the column and optimize the design of the structures and their seismic response [8–11]. Therefore, RBS have been largely used to guarantee strong column–weak beam behaviour, and many studies have been carried out to investigate their seismic behaviour [12–15]. In order to enhance the capacity of the welded connection and the ductility of the RBS joints, rib stiffeners have been also studied by the authors of [15,16], who verified the enhanced seismic performance of such stiffened RBS joints. Lee and Kim [17] also studied the seismic response of RBS joints with bolted web attachment and provided effective design criteria to promote a ductile response under seismic loading. Sofias and Pachoumis [18] tested two

RBS joints with extended endplate beam-to-column connection and European profiles, thus demonstrating the effectiveness of RBS application with European connections and steel profiles. Mousavi et al. [19] proposed an optimization design procedure of RBS joints using genetic algorithms. More recently, Onuralp and Bakır [20] performed a numerical study to investigate the seismic performance of novel replaceable RBS joints for steel moment-resisting frames. The concept of replaceable RBS joints also allows considering such detail as an alternative type of flexural damper for the mitigation of seismic effects in buildings that can be combined with other passive systems [21,22].

As it can be easily recognized, a large number of studies have been carried out to investigate the seismic performance and design of RBS joints. However, the response of seismically damaged RBS joints subjected to elevated temperature (e.g., the case of fire after an earthquake) has not been widely investigated, especially in the framework of Eurocode 8-compliant steel MRFs. Therefore, parametric finite element (FE) simulations have been carried to investigate such an open issue. In particular, a building archetype with perimeter steel MRFs was designed with welded and stiffened RBS joints according to Eurocodes and considered as reference case study. Both external and internal beam-to-column assemblies were sub-structured from the reference archetype. In particular, since no corner moment resisting bay was adopted, the external joints have a moment-resisting joint on one side of the column and a gravity load-resisting joint on the other side. Flush end-plate bolted connection was used for the gravity load-resisting joint. Different levels of seismic damage were imposed and three fire scenarios were considered.

This study is summarised in the present paper, which is organized as follows: (1) the first part describes the reference archetype and the considered loading scenarios; (2) modelling assumptions and their validation are given in the second part; (3) the results of FE simulations are summarised and discussed in the third part.

2. The Reference Archetype and the Considered Scenarios

2.1. Design Assumptions

The considered building archetype is a perimeter three-storey steel structure designed according to current structural Eurocodes [23–26]. The building has a rectangular plan with five bays in the long side and three bays in the short side (see Figure 1a), and all spans have the same length equal to 7 m; the interstorey height is equal to 3.5 m with the only exception of the first storey, whose height is 4.5 m.

Perimeter moment-resisting frames (MRFs) were placed in the longitudinal direction, while X-centrally bracing in the transverse direction (see Figure 1a). Figure 1b shows the vertical layout of the longitudinal side of the building, where it can be recognized that MRFs are located in the internal bays, and the outer bays are solely devoted to resist the gravity loads.

Dead and live loads were assumed to be equal to 5 kN/m^2 and 2 kN/m^2 , respectively. Peak ground acceleration (PGA) equal to 0.35 g, soil type C, and behaviour factor equal to 6.5 were also considered. The design seismic effects were evaluated by means of response spectrum analysis, also including the torsional effects. The interstorey drift limit at the damage limitation state was assumed to be equal to 0.75% of the interstorey height. The EC8 rules of the hierarchy of resistances were adopted considering as plastic zone the reduced beam sections, which were designed in accordance with EN1998-3 [25]. More details about the designed joints are given in Section 2.2. S355 steel grade was used for all members, and the profiles of columns and beams of the designed MRFs are summarized in Table 1.

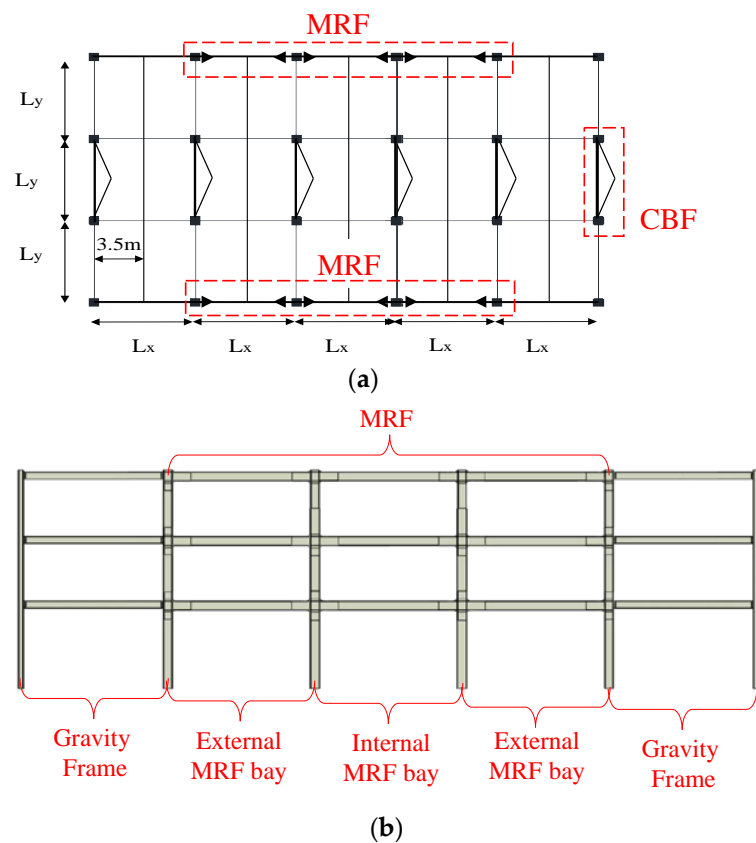


Figure 1. Moment-resisting frame (MRF) and concentrically braced frame (CBF) layout and main geometrical features of the building archetype (a) and Perimetral MRF (b) view.

Table 1. Cross section of the investigated moment-resisting frame.

Storey	Gravity Load Frame (Outer Bays)		External MRF Bays		Internal MRF Bay	
	Column	Beam	Column	Beam	Column	Beam
I	HEB300	IPE400	HEB 500	IPE500	HEB550	IPE500
II	HEB300	IPE400	HEB 500	IPE500	HEB550	IPE500
III	HEB300	IPE400	HEB 500	IPE500	HEB550	IPE500

2.2. Details of the Designed Beam-to-Column Joints

Figure 2a shows the details of the designed beam-to-column joints that were sub-structured from the reference building. The external joint of the MRF consists of a welded RBS connection on one side of the column (i.e., the connection of the MRF) and a flush end-plate bolted connection on the other side (i.e., the connection of the gravity load-resisting bay). The internal joint comprises two welded RBS connections per column side.

All beam-to-column connections were designed according to EN1993-1-8 [26], while the details of reduced beam sections were designed according to EN1998-3 [25]. In addition, RBSs were alternatively designed to provide two different levels of flexural resistance: (i) RBS with flexural resistance ($M_{RBS,Rd}$) equal to 80% of the beam plastic moment ($M_{pl,Rd}$) (hereinafter referred to as RBS-80) and (ii) RBS with $M_{RBS,Rd}$ equal to of $0.65 M_{pl,Rd}$ (hereinafter referred to as RBS-65).

The geometrical features of both the external and internal investigated RBS (i.e., a, b, c, and R) are depicted in Figure 2b and summarized in Table 2.

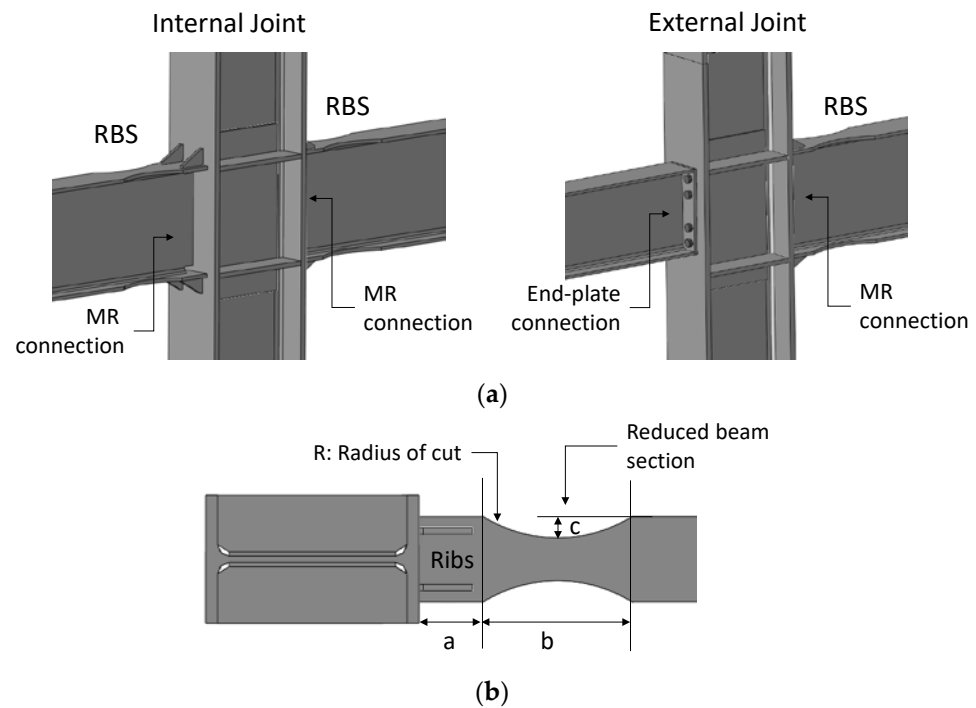


Figure 2. Moment-resisting (MR) and end-plate connection of both internal and external joints (a) and main geometrical features of the RBS connection (b).

Table 2. Features of the designed RBS.

Designed RBS	Geometrical Features					Flexural Resistance		
	a mm	b mm	c mm	R mm	Ze cm ³	M _{pl,Rd} kNm	M _{RBS,Rd} kNm	M _{RBS,Rd} /M _{p,Rd} -
RBS-80	150	350	30	525	1729	779	614	0.79
RBS-65	150	350	50	331	1419	779	504	0.65

The resistance of the rib-stiffened connection and the column web panel of the RBS joints were designed to resist the effects due to Equations (1) and (2), respectively.

$$M_{cf,Ed} = M_{RBS,Rd} + V_{RBS} \cdot e \tag{1}$$

$$M_{cc,Ed} = M_{RBS,Rd} + V_{RBS} \cdot \left(e + \frac{d_c}{2} \right) \tag{2}$$

where $M_{cf,Ed}$ and $M_{cc,Ed}$ are the design bending moment at the column face and at the column axis, V_{RBS} is the shear force in the reduced beam section, e is the distance between the beam plastic hinge and the column face, and d_c is the column depth.

In order to enhance the resistance of the welded connection and to prevent the yielding of the beam segment close to the column, double rib stiffeners were designed according to [15,16].

2.3. Investigated Loading Scenarios

The examined joints were investigated as follows: first cyclic loading and fire were separately applied; afterwards, fire was applied following cyclic loading. With this regard, the cyclic loading was imposed by means of AISC341 [27] protocol up to two levels of seismic-like damage, namely 0.04 rad (which may correspond to significant damage limit state) and 0.06 rad (for near collapse limit state), and three alternative fire scenarios were simulated as shown in Figure 3. Thus, 36 scenarios were considered on four different beam-to-column joints, as summarized in Table 3.

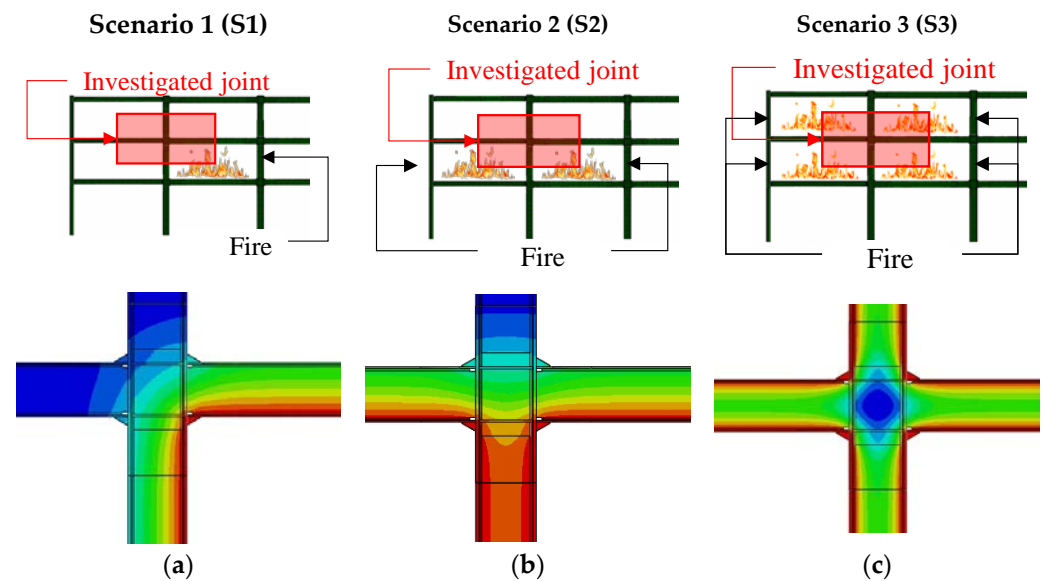


Figure 3. Considered fire scenarios, and examples of the corresponding temperature distribution within the investigated joints: S1 (a), S2 (b) and S3 (c).

Table 3. Investigated loadings and their combinations.

Beam–Column Assembly	RBS Resistance	Imposed Cyclic Damage	Fire Scenarios
External	80% $M_{pl,Rd}$	No damage (ND)	Only one bay (I)
Internal	65% $M_{pl,Rd}$	Significant damage (SD–0.04 rad)	Two lower bays (II)
		Near collapse (NC–0.06 rad)	All bays (III)
Total number of cases:			36

The joint assemblies were identified based on the following nomenclature:

- The configuration of the assemblies: “IJ” for the internal joints and “EJ” for the external joints.
- The flexural resistance of the RBS: “RBS-80” and “RBS-65” for RBS having plastic moments equal to 80% and 65% of the beam plastic moment, respectively;
- The imposed seismic damage: “ND” (no damage) for the joint subjected only to the fire loads, and “SD” or “NC” (significant damage and near collapse limit state, respectively) for the joints subjected to a cyclic loading up to 0.04 rad and 0.06 rad, respectively.
- The fire scenarios are identified as S1, S2, and S3, as shown in Figure 3.

For the sake of clarity, the identification code associated with an internal joint with resistance of RBS equal to 80% of the beam plastic moment, an imposed cyclic damage corresponding to 0.04 rad, and subjected to the second fire scenario is IJ-80%-SD-I.

The three investigated fire scenarios (i.e., S1, S2 and S3) are depicted in Figure 3, where the bay and the storey where the fire action is modelled are shown (see Figure 3a), and the corresponding distributions of the temperature within the steel joints are pointed out (see Figure 3b).

3. Finite Element Models

3.1. Modelling Assumptions

Finite element analyses (FEAs) were performed by means of Abaqus [28]. The adopted modelling assumptions are consistent with those presented by the authors of previous studies [29,30]. Therefore, only the main hypotheses are described hereinafter.

The FE models were discretized by means of structured meshes of C3D8I solid elements (i.e., 8-node linear brick, incompatible mode), as shown in Figure 4; “Tie constraints”

were adopted to model the welds, while normal and tangential contacts were modelled using “Hard contact” and “Penalty contact” formulations.

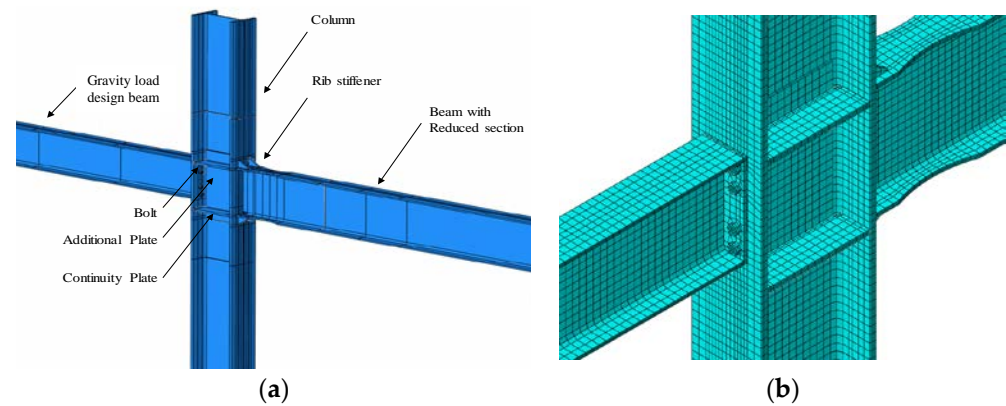


Figure 4. Main features of the FE model: geometry (a) and mesh (b).

The geometrical imperfections of the members were accounted for by imposing the scaled shape of the imperfection-like engine modes obtained from buckling analysis as described by the authors of [31].

European S355 steel grade was adopted for all the profiles and plates, while grade 10.9 was used for bolts. The expected mean yield stress of S355 was used through γ_{OV} factor equal to 1.25, as recommended by EN1998-1 [24], and combined hardening was modelled as in [3]. The non-linear behaviour of the bolts at ambient temperature was modelled as shown in [32,33].

The stress–strain curves at elevated temperatures were scaled through the reduction factors (k) for both structural steels and bolts as prescribed by EN 1993: 1–2 [34] (see Figure 5). The engineering curves in Figure 5 were converted into true stress–true strain curves and implemented in the FE models.

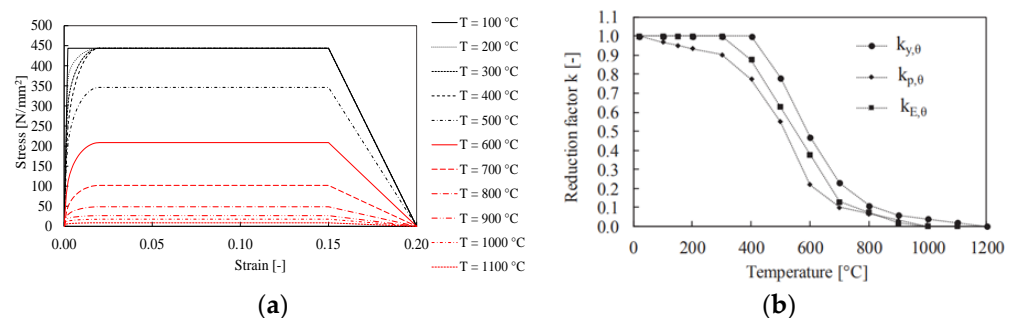


Figure 5. Stress–strain curves (a) and relevant reduction factors (b) at elevated temperatures.

Three analyses were performed per investigated joint, and each analysis comprised different intermediate steps as follows:

- Cyclic loading at ambient temperature (i.e., 20 °C): Step 1, clamping the bolts; Step 2, cyclic displacements imposed at the tip of the sub-assembled beam (the AISC341 [27] loading protocol has been used to simulate the seismic damage);
- Fire scenario on undamaged joints: Step 1, clamping the bolts; Step 2, application of gravity loads; Step 3, application of ISO834 curve [35] on the surfaces of the structural elements depending on the simulated fire scenario (heating time equal to 60 min);
- Fire scenario on cyclically damaged joints: Step 1, clamping the bolts; Step 2, cyclic displacements imposed at the tip of the sub-assembled beam; Step 3, application of gravity loads; Step 4, application of the fire scenario (heating time equal to 60 min).

In order to perform thermal analyses, a sequentially coupled thermal (transient) stress (implicit dynamic) analysis procedure was adopted; in particular, two sequential analyses were performed:

- Heat transfer: this was carried out to simulate the heat transfer from the external surface of the heated elements through their cross section and along their length.
- Stress analysis: this was carried out to simulate the structural responses of heated elements that are exposed to fire or thermal loading resulting from the previous step.

3.2. Validation of the FE Models

The accuracy of the adopted modelling assumptions at ambient temperature was verified against the experimental results from Brandon Chi and Chia-Ming Uang [8], who performed three cyclic tests on RBS joints whose main features are summarized in Table 4 (hereinafter, these specimens are identified as DC-1, DC2, and DC3).

Table 4. Features of the RBS joints tested in [8].

Specimen	Elements	Cross Section	Yield Strength [N/mm ²]	Tensile Strength [N/mm ²]	Elongation [%]
DC-1	Column	W27x146	344	433	46
	Beam	W36x150	359	445	47
DC-2	Column	W27x194	427	453	61
	Beam	W36x150	359	445	47
DC-3	Column	W27x194	375	482	30
	Beam	W27x194	427	453	61

Figure 6 depicts the comparison of the FE predictions and the experimental results from [8] in terms of moment vs. plastic rotation curves for all considered cases (i.e., DC1, DC2, and DC3 specimens).

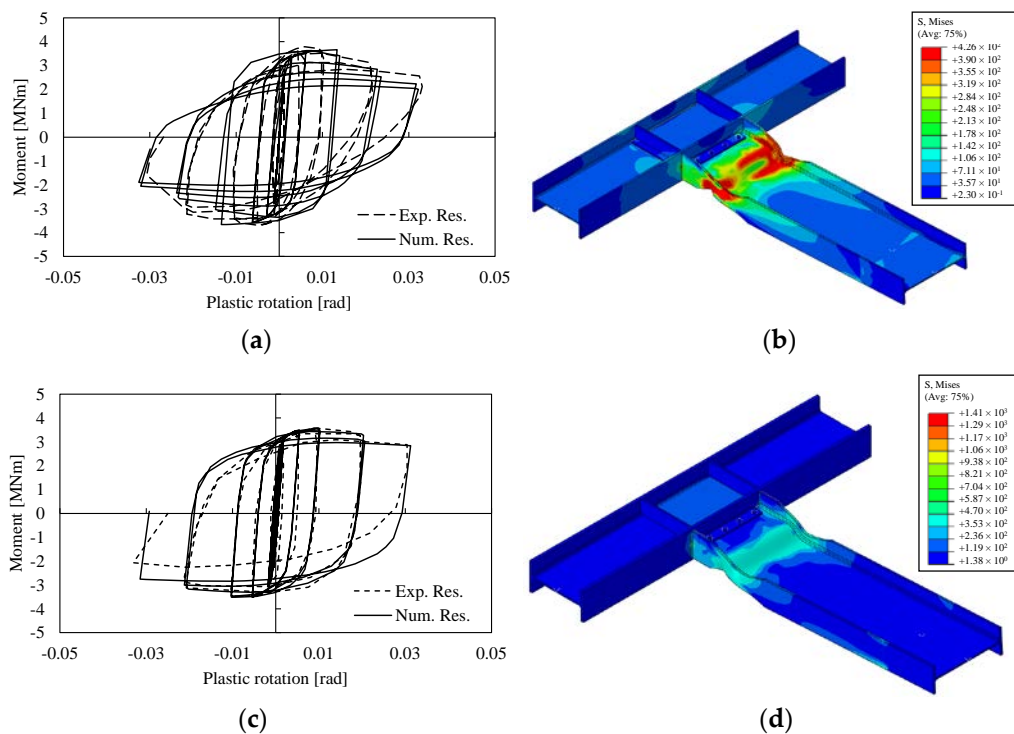


Figure 6. Cont.

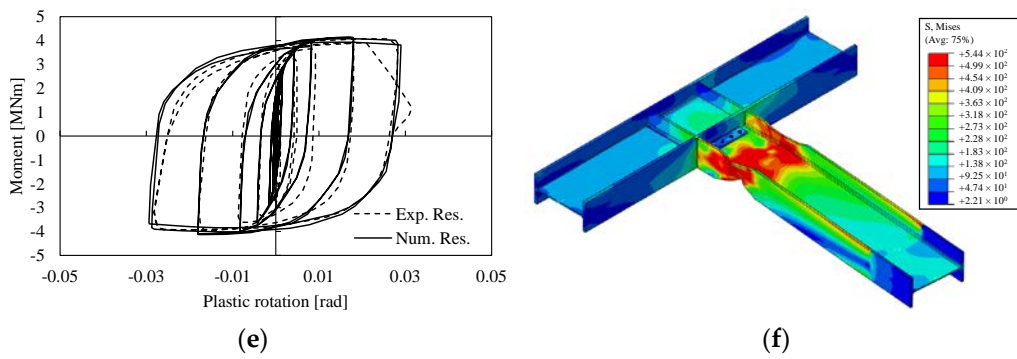


Figure 6. Comparison between the experimental [8] and numerical results in terms of moment–plastic rotation curves (a,c,e) and damage pattern (b,d,f) for all considered specimens tested in [8].

As can be observed in Figure 6, the FEM is able to mimic the experimental results in terms of moment–plastic rotation curves; moreover, the equivalent plastic deformations are consistent with the experimental damage pattern in [8].

To the a best of the authors’ knowledge, the results of fire tests on seismically damaged RBS joints are not available in the literature. Therefore, in this study, the same modelling assumptions adopted by Tartaglia et al. [3] were implemented. In fact, the FEM in [3] were validated against fire tests on steel joints, and their predictive accuracy is deemed satisfactory.

4. Results of Parametric FEAs

4.1. Seismic Behaviour

The results of both external and internal joints under cyclic loading at ambient temperature are depicted in Figure 7 in terms of moment–rotation curves (where the moment has been normalised to the plastic moment of the beam $M_{pl,Rd}$) and damage pattern, showing the distribution of the equivalent plastic deformations (PEEQ). For the sake of brevity, only the distribution of PEEQ of the joints is shown at 0.06 rad. As can be observed, the normalized response curves of RBS-80 and RBS-65 are very similar, although there is a difference in the width of the reduced beam flange.

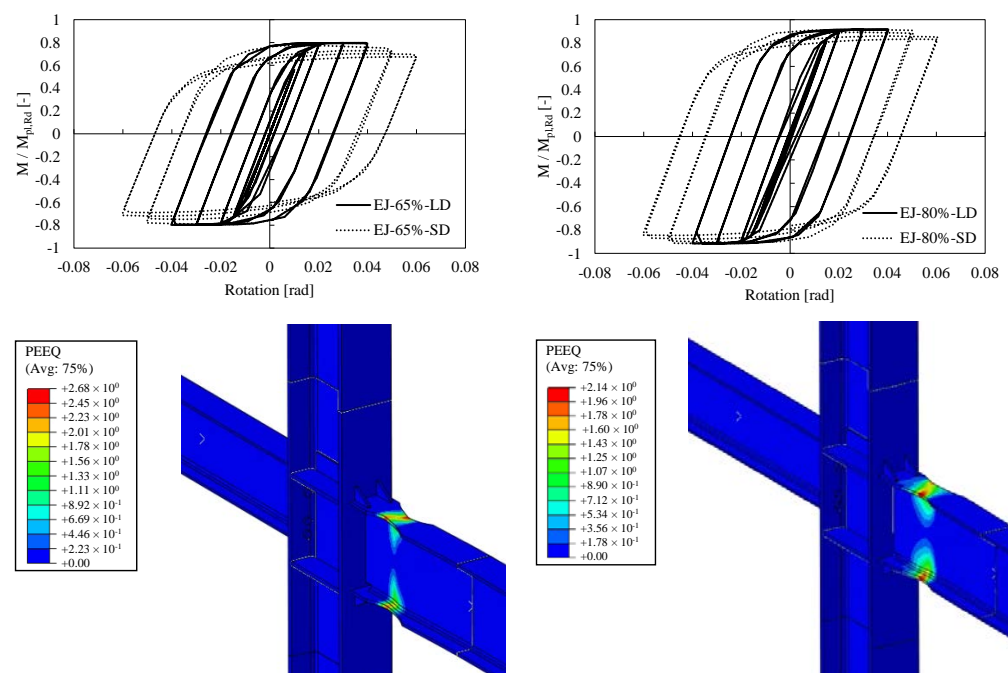


Figure 7. Cont.

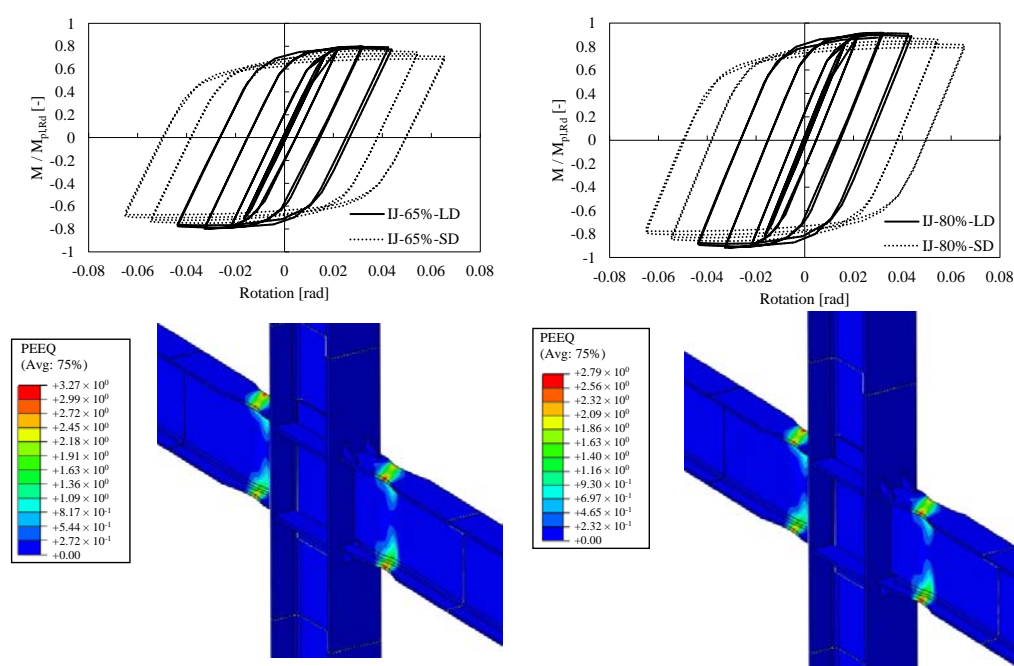


Figure 7. Cyclic behaviour of the investigated joints in terms of moment–rotation curves and equivalent plastic deformation (PEEQ).

All investigated joints show ductile behaviour (even at rotation of 0.06 rad), allowing the formation of the plastic hinge solely in the reduced portion of the beam. In addition, the presence of the two rib stiffeners contributes to preserving the connection components from plastic deformations, and the adoption of supplementary plates in the column panel zone contribute to keep that area in the elastic range.

Up to 0.04 rad, all joints do not exhibit degradation of their mechanical response curves, while degradation can be observed at 0.06 rad, which is mainly due to the activation of local buckling in the plastic zone of the reduced beams.

4.2. Fire Behaviour

The results of FEAs of the undamaged joints subjected to the three considered fire scenarios (S1, S2, and S3) are presented in terms of time–rotation and temperature–rotation curves in Figure 8, where the Von Mises stress distribution of the EJ-80%-ND-S2 and IJ-80%-ND-S2 joints are also depicted.

All temperature–rotation curves have an initial rotation before at ambient temperature, which corresponds to the rotation induced by the gravity loads (both dead and live loads).

As previously described, the external joints have an RBS connection on one side of the column, and a flush end-plate connection on the other side. This configuration is strongly influenced by fire loads. As depicted in Figure 8a,b, both external RBS-80 and RBS-65 s exhibit good behaviour in the S1 scenario up to 800 °C. In contrast, for S2 and S3, the flush end-plate connection experiences a significant reduction in resistance due to the large concentration of damage into the end-plate and first bolt row (see Figure 8e). In the case of RBS-80 in the S1 scenario, the stiffness degradation becomes evident when a temperature of 650 °C is reached at the lower flange of the beam (see Figure 8f).

The resistance of the RBS, namely the width of the cut flange, highly influences the fire behaviour of the joints. For instance, comparing the response of the EJ-RBS-80 and EJ-RBS-65 joints in the S1 scenario, it can be observed that the weaker the RBS, the worse its fire response (see Figure 9); indeed, the EJ-RBS-80 shows a good fire performance up to 55 min, while the corresponding RBS-65 shows a complete loss of stiffness after 38 min.

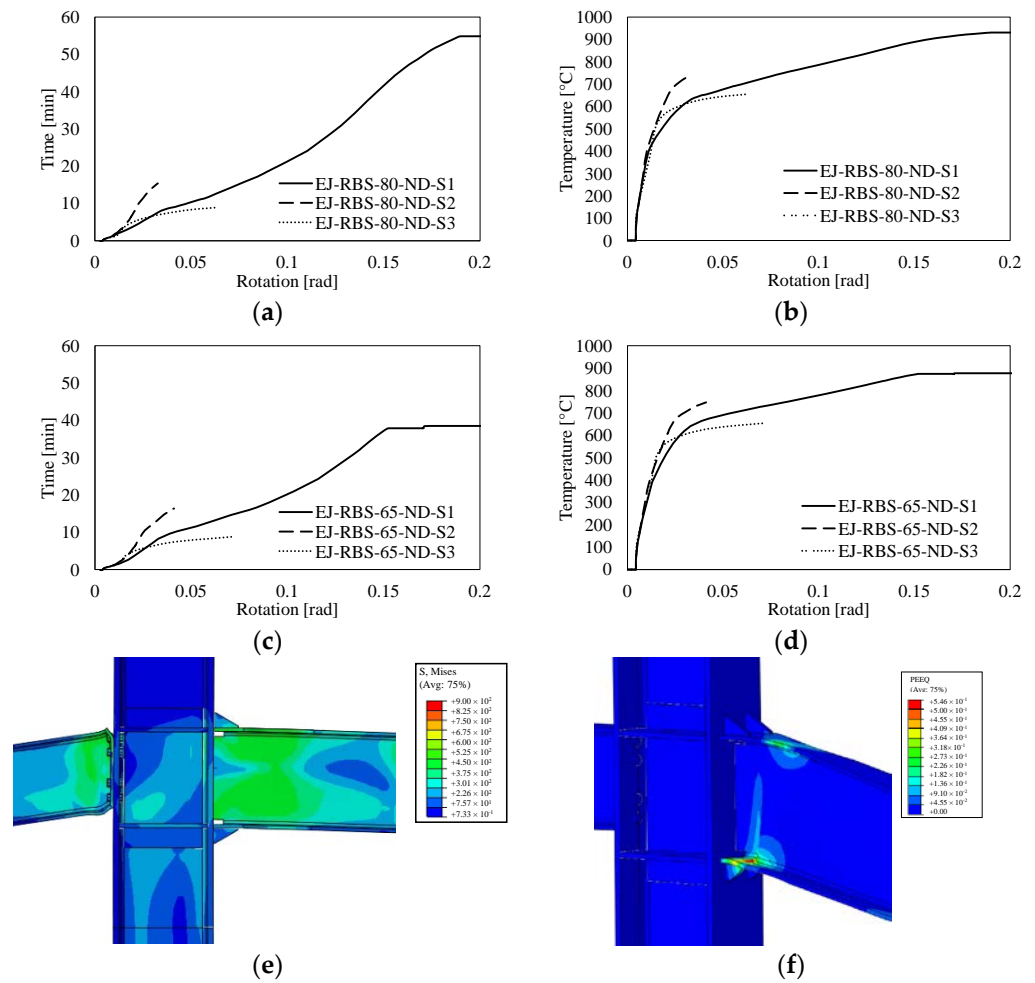


Figure 8. FE results of undamaged external joints subjected to elevated temperature in terms of time-rotation curves (a,c), temperature rotation curves (b,d) and Von Misses and PEEQ distribution (e,f).

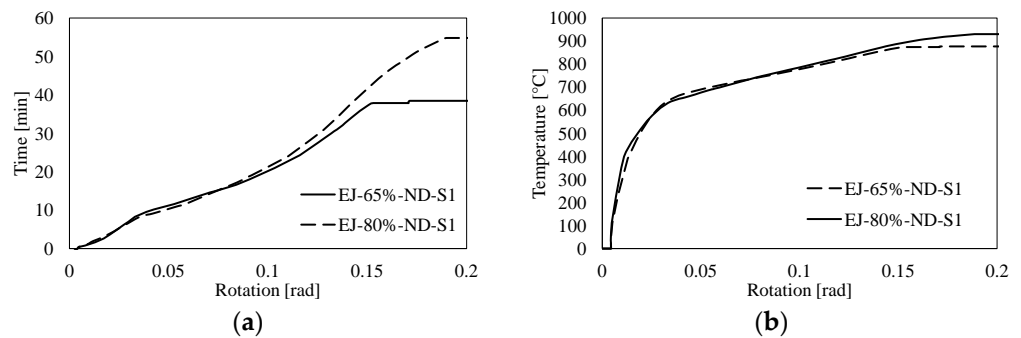


Figure 9. Comparison between the external RBS-65 and RBS-80 joints in terms of time-rotation (a) and temperature-rotation (b) curves.

The results of the internal joints are depicted in Figure 10. It should be observed that, in contrast to the external, the internal joints are symmetric, having the same connections and beams on both sides of the column. Therefore, only the results belonging to the right beam are pointed out hereinafter. Moreover, for the sake of brevity and since the results are perfectly comparable, only the results of the IJ-RBS-80 joints are presented.

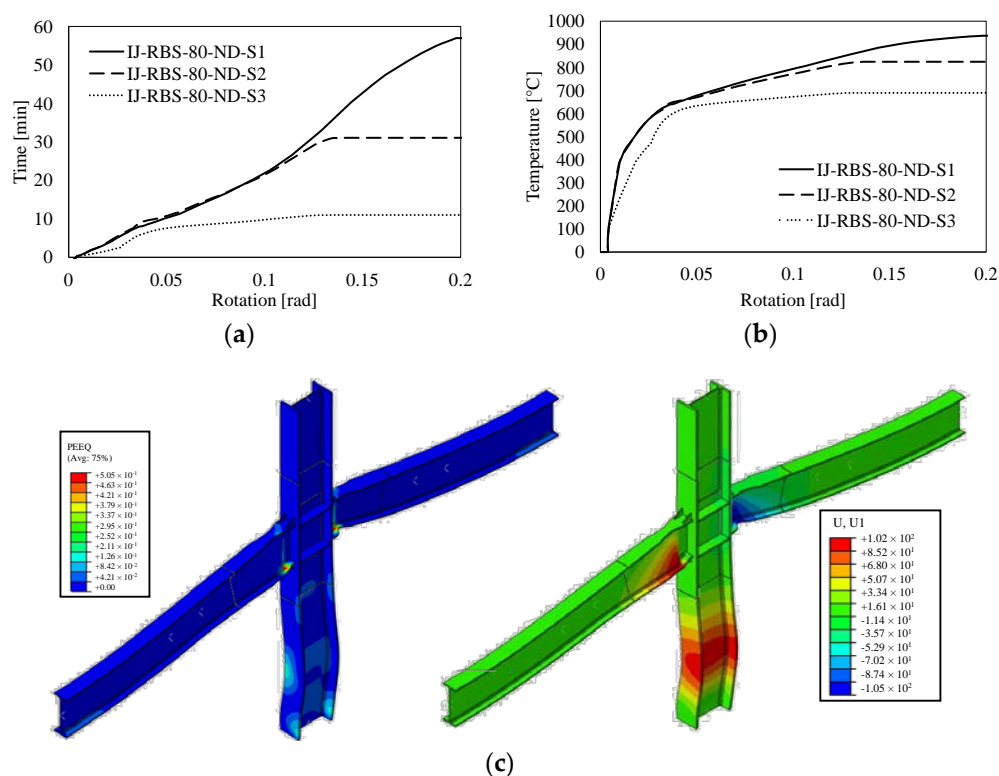


Figure 10. Results of the IJ-RBS-80 joints in terms of time–rotation curve (a), temperature–rotation curve (b) and PEEQ (c).

For the S1 scenario, the considerations made for the external joints can be extended, while a higher performance can be observed in the S2 and S3 scenarios (see Figure 10a,b).

As expected, since the beams and the connection are the same, the results of the S1 and S2 scenario are rather similar. However, increasing the temperature of the IJ-RBS-80-ND-S2 affected the loss of stiffness. This difference is due to the instability of the column that is subjected to fire on both sides in the S2 scenario (see Figure 10c).

In the case of the S3 scenario, the worst response for all examined cases can be observed. These results depend on the severity of the fire scenario, where elevated temperatures are applied throughout the surfaces of the assemblies.

4.3. Fire Behaviour of Seismically Damaged Joints

The fire performances of seismically damaged internal joints are depicted in Figure 11 in terms of time–rotation and temperature–rotation curves. In Figure 12, the distributions of PEEQ, temperatures, and Von Mises stresses of the IJ-RBS-65-NC are pointed out for S1, S2, and S3. Additionally, in these cases, due to the symmetry of the connections’ geometry and the applied loads, the results are solely shown for one side of the beam.

It is worth noting that similar to the undamaged joints, the FE results for the damaged RBS in S1 and S2 are similar, while the joints in S3 exhibit greater deterioration due to a substantial increase in temperature. In particular, it can be observed that after 10 min of exposure, the IJ-RBS-65-NC-S1/S2 experience a rotation of 0.05 rad, while the IJ-RBS-65-NC-S3 joints exhibit a rotation of 0.13 rad. Figure 12 confirms that all plastic deformations develop in the beam, while the connection and the column remain in the elastic range (Figure 12a,d,g). In addition, large plastic deformations as well as out of plane deformations can be observed in the lower part of the beam for the S1 and S2; in contrast, small deformations in the same parts of the beam occur in the case of S3 due to a more homogeneous distribution of the temperatures (see Figure 12b,c,e,f,h,i).

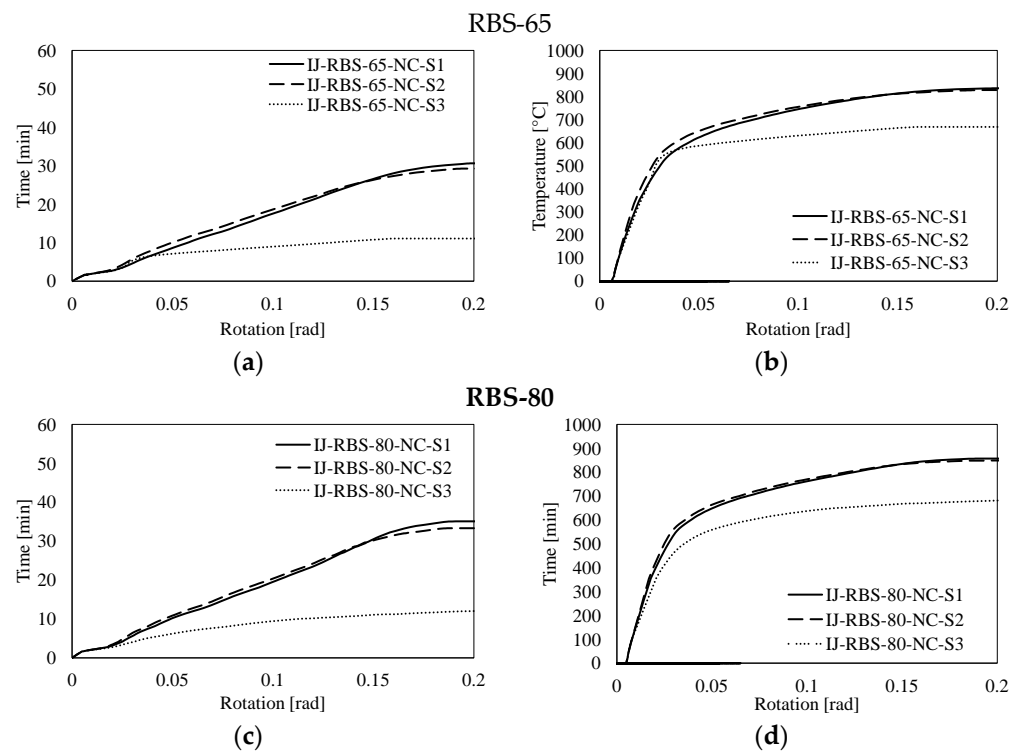


Figure 11. Time–rotation (a,c) and temperature–rotation (b,d) of the RBS-65/85 internal joints subjected to the S1–S3 scenarios.

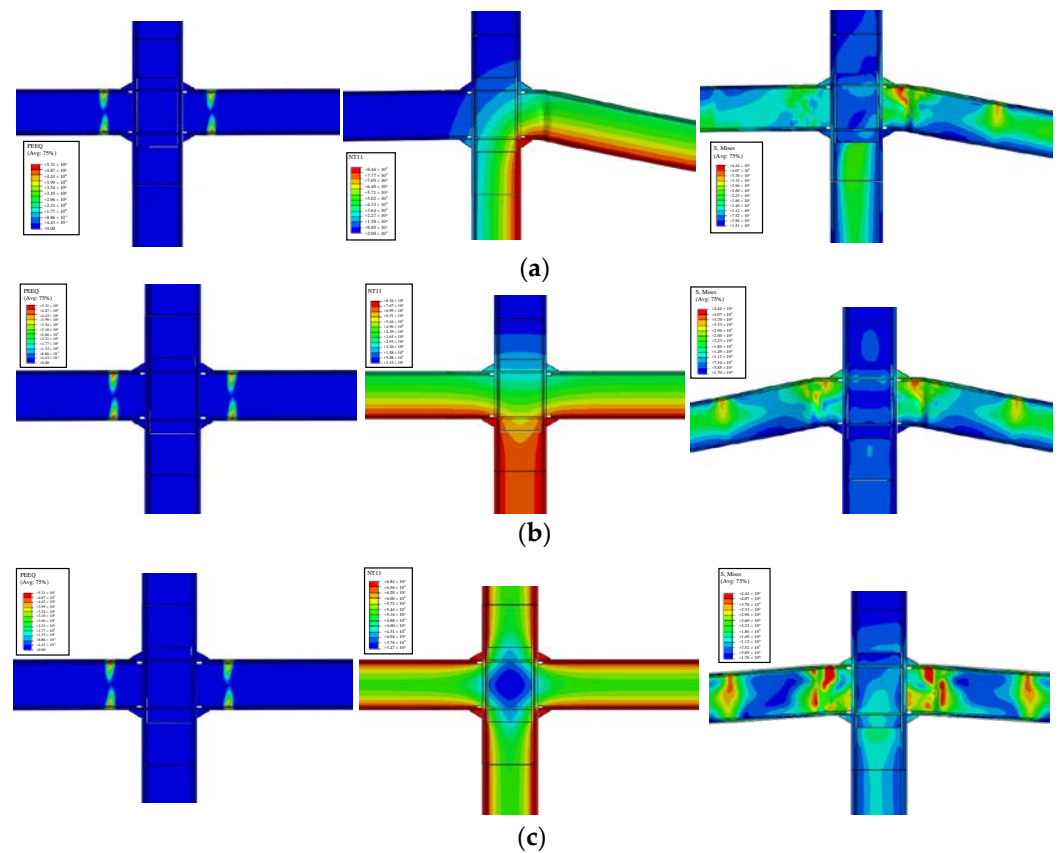


Figure 12. PEEQ, temperature, and Von Mises stress distributions of internal joints subjected to S1 (a), S2 (b), and S3 (c) fire scenarios.

Similar to the results depicted in Figure 9, it can be observed that the resistance of the RBS influences the fire performance of the joint. In fact, independently from the fire scenario (S1, S2, and S3), the RBS-80 joints reach a greater ultimate temperature and resist for a longer time than RBS-65 (see Figure 13).

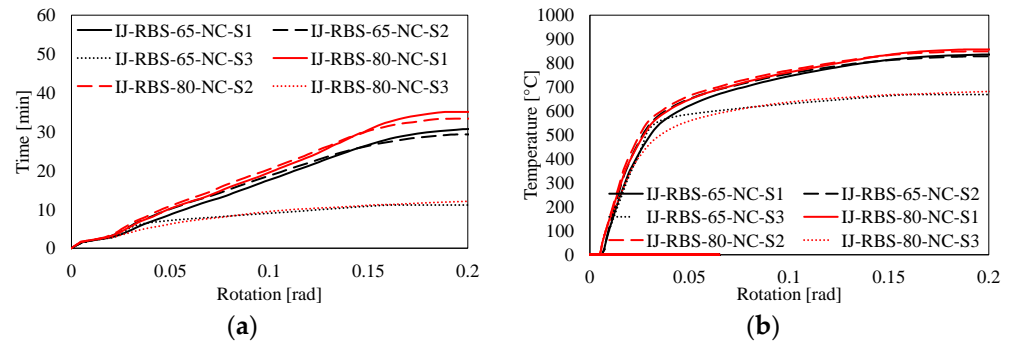


Figure 13. Comparison between the RBS configurations in the S1, S2, and S3 fire scenarios in terms of time-rotation (a) and temperature-rotation curves (b).

However, the difference between the RBS-80 and the RBS-65 is rather small. In fact, despite the seismic damage reducing the beam capacity, its entity marginally affects the fire performance of the joints since the seismic damage is mainly concentrated in the beam flanges, while the fire resistance is mainly influenced by the shear resistance of the beam, which is not impaired by the cyclic loading. This aspect is clarified in Figure 14, where the results of the undamaged joints are compared to those which are seismically damaged. It can be observed that the imposed cyclic damage reduces both the maximum resisting temperature and the resisting time, but such a reduction is not directly influenced by the cut of the RBS.

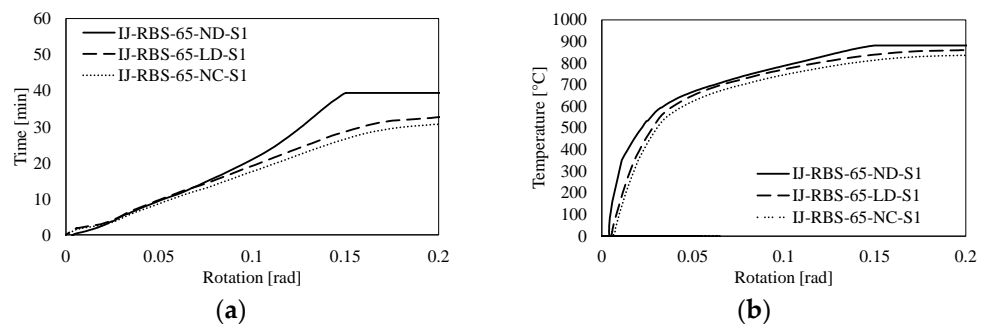


Figure 14. Influence of the cyclic pre-damage on the IJ-RBS-65 joints subjected to the S1 scenario in terms of time-rotation (a) and temperature-rotation curves (b).

5. Conclusions

The behaviour of steel welded reduced beam section (RBS) joints equipped with rib stiffeners subjected to elevated temperature was numerically investigated, also considering the effects of initial plastic damage induced by cyclic (seismic-like) loading. Both internal and external joints were considered, and two different sizes of the cuts for the beam flange were considered (namely RBS-65 and RBS-80, corresponding to 65% and 80% of the beam plastic moment). Based on the obtained results, the following conclusions can be summarized:

- The adopted finite element modelling assumptions satisfactorily simulate the mechanical response of the joints on the basis of the comparison with some experimental results available from the literature. In particular, the elastic stiffness, resistance, hysteretic response, and damage pattern are accurately predicted.
- All examined RBS joints show very ductile behaviour under cyclic loading; indeed, independently from the imposed ultimate rotation (4% and 6%), all plastic deforma-

tions are confined in the reduced segment of the beam. Moreover, the presence of the welded rib stiffeners allows the connection to be kept in the elastic range, thus preserving the beam-to-column welds from premature failure.

- As expected, the joints with the greater cut of the beam flange (i.e., RBS-65) exhibit larger degradation under cyclic loading due to out-of-plane plastic deformation at 0.06 rad.
- When exposed to fire, the undamaged joints with the greater cut of the beam flange (i.e., RBS-65) exhibit slightly greater degradation, but the differences are rather small in comparison with RBS-80. However, the stronger joints guarantee greater resisting time.
- The seismically damaged joints do not show appreciable differences if subjected to fire scenarios, since the cyclic pre-damage is mainly in the beam flanges, while the fire resistance is mainly guaranteed by the shear resistance of the beam, which is scarcely influenced by the seismic damage.

Author Contributions: Conceptualization, R.T., M.D. and R.L.; Software, R.T. and M.D.; Writing – original draft, R.T. and M.D.; Writing – review & editing, R.T., M.D. and R.L.; Supervision, R.L. All authors have contributed equally to this work. All authors have read and agreed to the published version of the manuscript.

Funding: This research received no funding.

Institutional Review Board Statement: Not applicable.

Data Availability Statement: The data presented in this study are available on request from the corresponding author.

Conflicts of Interest: The authors declare no conflict of interest.

References

1. Merouani, M.R.; Kada, A.; Lamri, B.; Piloto, P.A.G. Finite-element analysis for the performance of steel frames under fire after earthquake. *Asian J. Civ. Eng.* **2023**, *24*, 593–606. [\[CrossRef\]](#)
2. Risco, G.V.; Zania, V.; Giuliani, L. Numerical assessment of post-earthquake fire response of steel buildings. *Saf. Sci.* **2023**, *157*, 105921. [\[CrossRef\]](#)
3. Tartaglia, R.; D’Aniello, M.; Wald, F. Behaviour of seismically damaged extended stiffened end-plate joints at elevated temperature. *Eng. Struct.* **2021**, *247*, 113193. [\[CrossRef\]](#)
4. Bosco, M.; Tirca, L. A novel design criterion for I-shape beams of steel MRF buildings in subduction-zone earthquake-prone areas. *Structures* **2023**, *48*, 2098–2115. [\[CrossRef\]](#)
5. Barbagallo, F.; Bosco, M.; Ghersi, A.; Rossi, P.P. A Strength Amplification Factor to Counterbalance P- Δ Effects in Steel Moment Resisting Frames. *Lect. Notes Civ. Eng.* **2022**, *262*, 1048–1055.
6. Barbagallo, F.; Bosco, M.; Ghersi, A.; Marino, E.M.; Rossi, P.P. Seismic assessment of steel MRFs by cyclic pushover analysis. *Open Constr. Build. Technol. J.* **2019**, *13*, 12–26. [\[CrossRef\]](#)
7. Georgescu, D. Recent developments in theoretical and experimental results on steel structures: Seismic resistant braced frames. *Costr. Met.* **1996**, *1*, 39–52.
8. Chi, B.; Uang, C.M. Cyclic Response and Design Recommendations of Reduced Beam Section Moment Connections with Deep Columns. *J. Struct. Eng.* **2002**, *128*, 464–473. [\[CrossRef\]](#)
9. Montuori, R. The influence of gravity loads on the seismic design of RBS connections. *Open Constr. Build. Technol. J.* **2014**, *8*, 248–261. [\[CrossRef\]](#)
10. Montuori, R. Design of “Dog-bone” connection: The role of vertical loads. In Proceedings of the COMPDYN 2015–5th ECCOMAS Thematic Conference on Computational Methods in Structural Dynamics and Earthquake Engineering, Crete Island, Greece, 25–27 May 2015; pp. 3368–3387. [\[CrossRef\]](#)
11. Montuori, R.; Sagarese, V. The use of steel rbs to increase ductility of wooden beams. *Eng. Struct.* **2018**, *169*, 154–16115. [\[CrossRef\]](#)
12. Rahnavard, R.; Hassanipour, A.; Siahpolo, N. Analytical study on new types of reduced beam section moment connections affecting cyclic behavior. *Case Stud. Struct. Eng.* **2015**, *3*, 33–51. [\[CrossRef\]](#)
13. Sofias, C.; Kalfas, C.; Pachoumis, D. Experimental and FEM analysis of reduced beam section moment endplate connections under cyclic loading. *Eng. Struct.* **2014**, 320–329. [\[CrossRef\]](#)
14. Bompa, D.; Elghazouli, A.Y. Seismic behaviour and design of steel reduced beam section connections. In Proceedings of the SECED 2019 Conference London, London, UK, 9–10 September 2019.
15. Lee, C.; Jung, J.; Oh, M.; Koo, E. Experimental study of cyclic seismic behaviour of steel moment connections reinforced with ribs. *J. Struct. Eng.* **2005**, *131*, 108–118. [\[CrossRef\]](#)

16. Lee, C.H. Seismic design of rib-reinforced steel moment connections based on Equivalent Strut Model. *J. Struct. Eng.* **2002**, *128*, 1121–1129. [[CrossRef](#)]
17. Lee, C.H.; Kim, J.H. Seismic design of reduced beam section steel moment connections with bolted web attachment. *J. Constr Steel Res.* **2007**, *63*, 522–531. [[CrossRef](#)]
18. Sofias, C.E.; Pachoumis, D.T. Assessment of reduced beam section (RBS) moment connections subjected to cyclic loading. *J Constr Steel Res.* **2020**, *171*, 106151. [[CrossRef](#)]
19. Mousavi, S.E.; Mosalman Yazdi, H.A.; Mosalman Yazdi, M. Optimization Design of Reduced Beam Section Using Genetic Algorithm. *Int. J. Steel Struct.* **2022**, *22*, 805–815. [[CrossRef](#)]
20. Onuralp Özkılıç, Y.; Bakır Bozkurt, M. Numerical validation on novel replaceable reduced beam section connections for moment-resisting frames. *Structures* **2023**, *50*, 63–79. [[CrossRef](#)]
21. Wang, L.; Shi, W.; Zhou, Y. Adaptive-passive tuned mass damper for structural aseismic protection including soil–structure interaction. *Soil Dyn. Earthq. Eng.* **2022**, *158*, 107298. [[CrossRef](#)]
22. Wang, L.; Nagarajaiah, S.; Shi, W.; Zhou, Y. Seismic performance improvement of base-isolated structures using a semi-active tuned mass damper. *Eng. Struct.* **2022**, *271*, 114963. [[CrossRef](#)]
23. *EN 1993:1-1*; Eurocode 3: Design of Steel Structures–Part 1-1: General Rules and Rules for Buildings. CEN: Brussels, Belgium, 2005.
24. *Eurocode 1998-1*; Design of Structures for Earthquake Resistance. Part 1: General Rules, Seismic Actions and Rules for Buildings. European Committee for Standardization: Brussels, Belgium, 2005.
25. *Eurocode 1998-3*; Design of Structures for Earthquake Resistance–Part 3: Assessment and Retrofitting of Buildings. European Committee for Standardization: Brussels, Belgium, 2005.
26. *Eurocode 1993:1-8*; Design of Steel Structures. Part 1.8: Design of Joints. European Committee for Standardization: Brussels, Belgium, 2005.
27. *ANSI/AISC 341-16*; Seismic Provisions for Structural Steel Buildings. AISC (American Institute of Steel Construction): Chicago, IL, USA, 2016.
28. Dassault. *Abaqus 6.14—Abaqus Analysis User’s Manual*, Dassault Systèmes Simulia Corp; Dassault: Velizy-Villacoublay, France, 2014.
29. Tartaglia, R.; Milone, A.; D’Aniello, M.; Landolfo, R. Retrofit of non-code conforming moment resisting beam-to-column joints: A case study. *J. Constr. Steel Res.* **2022**, *189*, 107095. [[CrossRef](#)]
30. Tartaglia, R.; Milone, A.; Porta, A.M.; Landolfo, R. Seismic Retrofitting of Existing Industrial Steel Buildings: A Case-Study. *Materials* **2022**, *15*, 3276. [[CrossRef](#)] [[PubMed](#)]
31. Tartaglia, R.; D’Aniello, M.; Rassati GASwanson, J.A.; Landolfo, R. Full strength extended stiffened end-plate joints: AISC vs recent European design criteria. *Eng. Struct.* **2018**, *159*, 155–171. [[CrossRef](#)]
32. D’Aniello, M.; Cassiano, D.; Landolfo, R. Monotonic and cyclic inelastic tensile response of European preloadable GR10.9 bolt assemblies. *J. Constr. Steel Res.* **2016**, *124*, 77–90. [[CrossRef](#)]
33. D’Aniello, M.; Cassiano, D.; Landolfo, R. Simplified criteria for finite element modelling of European preloadable bolts. *Steel Compos. Struct.* **2017**, *24*, 643–658.
34. *Eurocode 1993:1-2*; Design of Steel Structures. Part 1.2: General Rules–Structural Fire Design. European Committee for Standardization: Brussels, Belgium, 2005.
35. *ISO 834-10:2014*; Fire Resistance Tests—Elements of Building Construction—Part 10: Specific Requirements to Determine the Contribution of Applied Fire Protection Materials to Structural Steel Elements. International Organization for Standardization: Geneva, Switzerland, 2014.

Disclaimer/Publisher’s Note: The statements, opinions and data contained in all publications are solely those of the individual author(s) and contributor(s) and not of MDPI and/or the editor(s). MDPI and/or the editor(s) disclaim responsibility for any injury to people or property resulting from any ideas, methods, instructions or products referred to in the content.